IEEE Access
Multidisciplinary | Rapid Review | Open Access Journal

SPECIAL SECTION ON CHALLENGES AND ENDEAVORS OF RADIATED RADIO FREQUENCY TESTS FOR 5G RADIOS

Received January 31, 2021, accepted February 9, 2021, date of publication February 22, 2021, date of current version March 1, 2021.

Digital Object Identifier 10.1109/ACCESS.2021.3060860

5G mmW Link Range Uncertainties From RF System Calculations and OTA Measurements

MARKO E. LEINONEN, (Member, IEEE), NUUTTI TERVO, (Member, IEEE), MARKKU JOKINEN, OLLI KURSU, AND AARNO PÄRSSINEN, (Senior Member, IEEE)

Center of Wireless Communications, University of Oulu, 90570 Oulu, Finland

Corresponding author: Marko E. Leinonen (marko.e.leinonen@oulu.fi)

This work was supported in part by the Academy of Finland 6Genesis Flagship under Grant 318927, in part by the Business Finland-funded 5G Finnish Open Research Collaboration Ecosystem (5GFORCE), and in part by the Business Finland-funded 5GViima.

ABSTRACT Phased arrays in 5G millimeter wave (mmW) communication are used at both link ends to separate users and to enhance the link range. The radio hardware's RF performance metrics vary due to part-to-part variations within component tolerances. In this paper, we derive probability density functions (PDFs) of over-the-air (OTA) transmission (TX) powers for individual transmitter (Tx) paths and total TX power of the 5G mmW array using Monte Carlo simulations based on component tolerances. The PDF of the TX power individual path of the array follows a log-normal distribution on a linear scale. Hence, the total array's OTA TX power is a sum of independent linear scale log-normal powers when the power combination happens in OTA towards the main beam direction. We show that the Tx array's mean power increases when multiple log-normally variated individual TX powers are summed together. Additionally, we prove that a link budget maps to a link range in a non-linear way, skewing the normally distributed link budget to a log-normally distributed link range. The link ranges based on RF system parameter analysis, RF system calculation, and OTA measured system error vector magnitude (EVM) based link range estimation had an excellent match when a 16-QAM 5G NR signal was used. The calculated link ranges are 410 and 434 meters, while the OTA measured system EVM measurement-based link range is 415 meters. For example, uncalibrated Tx array paths would increase the mean of the array's TX power by 1.2 dB, and the link range increases from 415 to 498 meters, but simultaneously the standard deviation increases from 26 to 51 meters.

INDEX TERMS Array receiver, array transmitter, error vector magnitude (EVM), phased array, probability density function, receiver sensitivity, system EVM.

I. INTRODUCTION

PARstartLink range in 5G millimeter-wave (mmW) systems is enhanced by utilizing steerable antenna arrays at both transmitter (Tx) and receiver (Rx) sides. 5G mmW systems will be used for backhaul and fronthaul links, mobile user communications, or an integrated backhauling operation as shown in Fig. 1. The first 5G mmW networks utilize lower frequency LTE or 5G network for signaling purposes and mmW frequencies for data transportation [1]. The integrated backhauling function, where a radio network unit acts as a proxy for the signal, will be included in the 3rd Generation Partnership Project (3GPP) 5G new radio (NR) standard release 16 [2], which is illustrated in Fig. 1.

The associate editor coordinating the review of this manuscript and approving it for publication was Wei Fan.

All regulatory and RF performance measurements for 5G mmW radios are performed over-the-air (OTA) for both user equipment (UE) [3] and base station (BTS) units [4] according to the 3GPP NR standards. Conducted measurements of array transmitter or receiver are impractical with large antenna arrays due to cabling complexity, high integration level, and a lack of conductive interfaces to all radio transceiver RF inputs. Examples of highly integrated 5G mmW transceivers are presented in [5]–[8] and a discrete component-based transceiver for mobile backhaul in [9].

The OTA measured an effective isotropic radiated power (EIRP) of the array Tx has uncertainty due to the variations caused by multiple sources. Hence, EIRP may vary even several dBs, which directly impacts the link range and the cell coverage of the 5G mmW system. The overall array EIRP is a combination of the conducted transmission (TX)

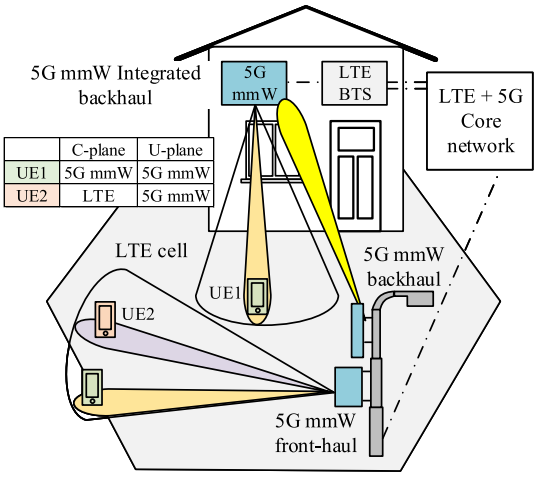

FIGURE 1. 5G mmW network topologies.

power, the gain of antenna element or antenna array, and the reproducibility and repeatability (R&R) of the OTA measurement [10]. Hence, each component in each signal path has an impact on the overall EIRP. Additionally, Rx variations such as gain, noise figure, and antenna array gain variation are included in the combined link range variation.

The minimum and the maximum requirements for the 5G mmW UE and BTS are given in the standards [3], and [4], respectively. However, these standard requirements do not specify the allowed maximum variation between devices. The product-to-product variation needs to be understood in depth by the device manufacturer since the variation reduces the production yield. If the standard defines only one limit, then the device manufacturer can set its design target based on the estimated or the measured variation of prototypes or products. The design target for the component or antenna array needs to be above the acceptance limit, and the design target can be set based on the expected quality level or a probability of products not complying with the specifications [11].

Accurate quality level estimation requires that the probability density function (PDF) of the radio parameter is known either based on simulations and measurements of prototypes or, preferably, based on a set of measurements of mass production samples. Similarly, radio link range estimation should be done based on known PDFs of parameters so that the link range or the coverage area of the cell can be accurately modeled. A 5G mmW radio link range estimation based on short-range measurements is presented in [12].

The paper is organized as follows. Section II presents statistical distributions used to model the radio parameters. Section III presents the proof-of-concept (PoC) 5G backhaul radio used for validation measurements and measured PDFs of radio parameters from the array transceiver. Additionally, section III includes the analysis of the PDFs which have the most significant contributions for the link range or the total array TX power, a noise figure (NF) of the array Rx, and the Rx array's coherence gain. Section IV focuses on a link range estimation and associated variations, and the conclusion is presented in Section V.

II. STATISTICAL DISTRIBUTIONS IN RF SYSTEM DESIGN

Paying attention to the shape of an RF parameter's PDF is essential already in the design phase of the radio, when block and component specifications are derived from the system level targets [13]. A normal distribution is the most commonly used statistical distribution to model variability in quality engineering [14], applied statistics [21] and automotive industry [22]. The normal distribution has the following advantages: it is symmetrical distribution defined with all real values, the variances are additive, and a sum of multiple independent normally distributed variables follows the normal distribution [21], [22]. In general, a sum of two or more independent random variables is the convolution of PDFs of their distributions [21].

Other commonly used distributions to model the variability are the uniform distribution, the log-normal distribution, and the truncated normal distribution [23]. The truncated normal distribution is used for screened components, where the components that do not meet the specification are removed, and thus the remaining tail of the distribution is truncated. The uniform distribution is used as a worst-case distribution to model the wear-out or aging components with a performance shift over the specification limits.

Gains of RF components are typically expressed on the dB scale [24]–[26], which is most convenient for the analysis purpose, and thus the variation is also defined on the dB scale. Hence, in the Tx signal chain analysis, the overall gain is a summation of the gains of individual components in the signal path. Thus, the Tx power analysis follows independent random number summation when discrete signal chain components are used, as done, for example, in [9]. The used components are manufactured in different processes, which ensures the independence of variations between components. If a variable follows a normal distribution on the dB scale, then the variable follows a log-normal distribution on a linear scale. In general, component validation measurements and data analysis should be done on the same scale used in the component specification to avoid scaling and interpretation problems.

Whereas in the individual Tx signal paths, the gains are additive on the dB scale, in parallel paths, the signals are summed on the linear scale. Hence, the EIRP of the TX array constructed by the parallel paths cannot be easily analyzed on the dB scale. Let us assume that a X, e.g., a gain of an amplifier on dB scale, is normally distributed. Then, on a linear scale, X can be written as

$$Y = 10^X, \tag{1}$$

where Y is log-normally distributed. The different base number, e.g., e, does not change the shape of the distribution, but it scales the PDF. Similarly, if the TX power level follows a normal distribution on dBm, the TX power follows a log-normal distribution on the mW scale.

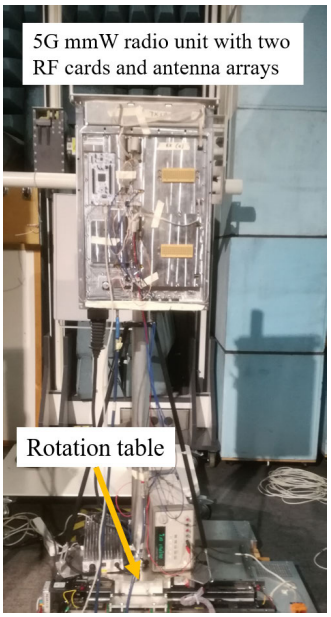

FIGURE 2. 5G mmW backhaul radio transceiver unit in EMC chamber on rotation table.

The log-normal distribution shape parameters, i.e. the mean μ and the standard deviation σ, can be calculated as

$$\mu = \log_e\left(m^2/\sqrt{(s^2+m^2)}\right) \text{ and} \tag{2}$$

$$\sigma = \sqrt{\log_e\left(s^2/m^2+1\right)}, \tag{3}$$

where m and s^2 are the mean and the variance of the normal distribution [23]. It can be seen from Eqs. (2) and (3) that both the mean (m) and the standard deviation (s) of normal distribution affect the overall shape of the log-normal distribution. If either m or s is increased in Eqs. (2) and (3), then both log-normal distribution parameters, the mean μ and the standard deviation σ, are increased. Hence, a large standard deviation of the normal distribution shifts the mean of the log-normal distribution significantly.

III. IMPLEMENTED 5G mmW RADIO UNIT FOR 28 GHz

A mobile 5G mmW backhaul proof-of-concept (PoC) radio unit to support 3GPP 5G NR band n257 (26.5 - 29.5 GHz) [4] has been designed and implemented, as shown in Fig. 2, and it was publicly demonstrated in the 2018 Winter Olympics in South Korea. The radio unit has two radio cards, and the RF block diagram of one radio card is shown in Fig. 3. The RF solution supports a time-division duplex (TDD) with RF switches that connect transmission and reception paths to a common antenna port located in the Tx/Rx front-end. The radio card includes 16 Tx and Rx chains, and each Tx-Rx chain pair is equipped with a shared 5-bit digitally controlled phase shifter to steer the radiated signal from the array towards the direction of interest [12].

A block chart of the mmW transceiver is depicted in Fig. 3. The RF architecture is a super-heterodyne with

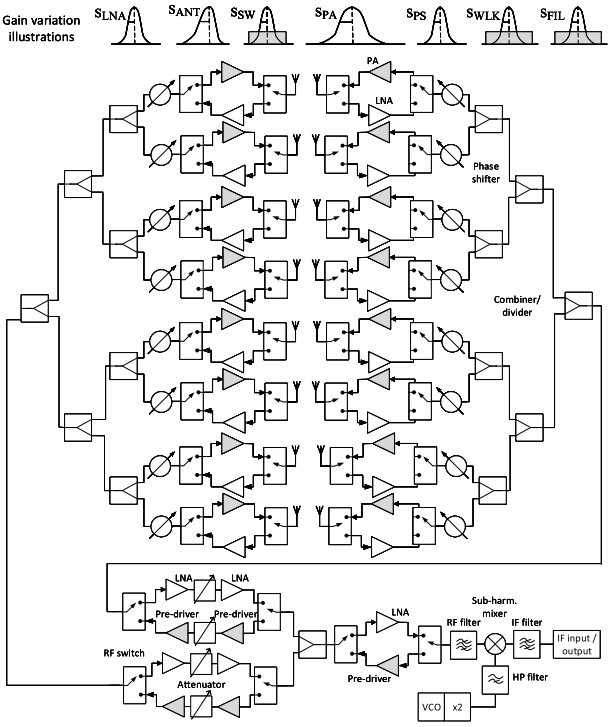

FIGURE 3. RF block diagram of 5G mmW proof-of-concept radio with illustrations of gain variations.

an intermediate frequency (IF) of 4 GHz. A low-side sub-harmonic gallium arsenide (GaAs) mixer [24] is used in both Rx and Tx. The common signal path for all chains in reception (RX) and TX modes includes frequency conversion, band-pass filtering of the mmW frequency band, low-pass filtering at IF, and power/gain control for TX and RX signals. Packaged Wilkinson power dividers at mmW frequency performed the RF power division, and combination [25]. The used low noise amplifiers (LNAs) in the Rx are surface-mounted devices (SMD), while the RF switches, phase shifters, and the RF power amplifiers (PAs) are bare die components [26]. All die components were connected to the printed circuit board (PCB) with bond wires.

The PDFs of the different components used in the system level calculations are illustrated at the top of Fig. 3. The RF array component variations have been modeled with normal, reverse log-normal and uniform distributions. The modeling PDFs and component specification limits (SL) have been selected based on the component data sheets and the measurement results.

The modeling PDFs have been scaled to the component limits with an assumption that the component is mass-produced with a process capability index $\boldsymbol{C}_{\mathrm{pk}}$ value of 1.0, which is considered to be the minimum limit for a high-volume product [14]. If the parameter follows the normal distribution, the $\boldsymbol{C}_{\mathrm{pk}}$ value 1.0 corresponds to a situation where the closest SL is three standard deviation units away from the mean value of the distribution [14]. For this reason,

the C_{pk} of 1.0 can be considered a worst-case analysis, since typical target for a mass-production component quality level is 1.33 or even 1.50 [14]. The C_{pk} of 1.50 corresponds a case, where the closest SL is four and half standard deviation units apart from the mean, which is considered as a Six Sigma-quality level [14]. The C_{pk} of 1.0 corresponds to a manufacturing loss of 1350 ppm while the C_{pk} of 1.50 has only 3 ppm, i.e. 3 products out of 1 million are defected.

The OTA measurements were performed in the EMC chamber (dimensions: 10 m × 6 m × 5 m, length, width, height, respectively) of the University of Oulu. It is larger than the 3 m chamber required for LTE system EMC testing [15]. The block diagram of the used OTA measurement arrangement is shown in Fig. 4.

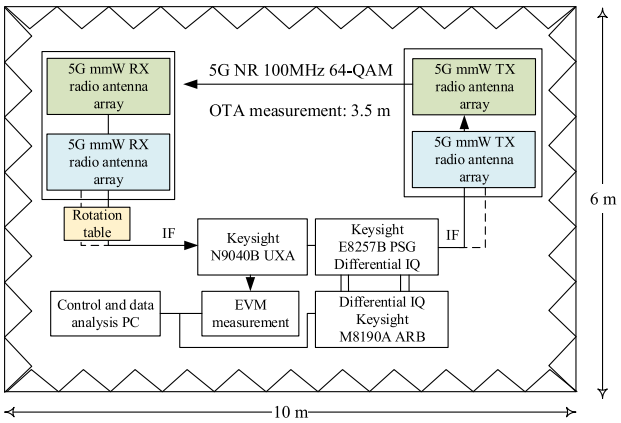

FIGURE 4. Block diagram of the implemented 5G mmW radio platform OTA measurement setup in EMC chamber.

The used OTA measurement arrangement is a direct far-field system. Similar systems are presented, e.g., in [17]–[20]. The measurement is performed in the antenna array's far-field condition, the DUT is rotated, and measurements are done with a fixed measurement antenna and position. The radio units were positioned 3.5 m apart and directly facing each other. The units are in the far-field of the antenna array since the threshold is 1.8 m [16]. The measured unit was rotated during OTA measurements while the measuring unit was in a fixed position. Only one of two radio cards of each unit was used during the OTA measurements. The free-space path loss in the OTA measurement was 72.3 dB at 28 GHz.

A. UN-CALIBRATED TX POWER OF TX ARRAY

The beam direction of the phased array in TX or RX modes can be steered towards the angle of interest Θ_s from the broadside of the array in the far-field with a progressive phase shift $\Delta\phi$ over the linear array, calculated as

$$\Delta\phi = \left(\frac{2\pi \cdot \sin\Theta_s \cdot d}{\lambda}\right), \tag{4}$$

where d is the spacing between the antenna elements and λ is the wavelength of the carrier [27]. The phase-shifted signals of the individual transmission paths are coherently combined in the air in TX mode. In the RX mode, the signal combination is done with discrete RF components in the 5G backhaul unit [9], where the non-idealities of the RF components will limit the achieved RX coherence gain [28].

The TX output signal level from an individual Tx path can be calculated as a summation of the individual component gains on dB scale as

$$P_{\text{out}} = \sum_{i=1}^{K} G_i + P_{\text{in}}, \tag{5}$$

where P_{in} is the input power of the Tx signal chain and G_i is the gain of the i^{th} component in the Tx path and the K is a total number of components in the Tx signal chain. If the gain (dB) of each Tx component is assumed to be normally distributed, the variance of the TX power of each individual Tx path can be calculated as [22]

$$\sigma^2_{P_{\text{out}}} = \sum_{i=1}^{K} \sigma_i^2, \tag{6}$$

where σ_i is the standard deviation of gain (dB) of the i^{th} component in the individual TX signal chain.

If the TX power of k^{th} Tx array path follows normal distribution on the dB scale, i.e.,

$$P_{\text{out},k} = N(P_{\text{out},k}, \sigma_k^2), \tag{7}$$

then the TX power of the k^{th} path on mW scale can be expressed as

$$P_{\text{lin},k} = 10^{\left(\frac{P_{\text{out},k}}{10}\right)} \tag{8}$$

and the $P_{\text{lin},k}$ follows a log-normal distribution, whose mean and standard deviation can be calculated with Eqs. (2) and (3), respectively.

The total TX power transmitted by the TX array toward the desired direction with a perfect signal combination in the air, is a summation of TX powers from all paths on linear scale and can be written as

$$P_{\text{lin,tot}} = \sum_{k=1}^{M} P_{\text{lin},k}, \tag{9}$$

where M is the number of transmission signal paths in the TX array and the total TX linear power follows the log-normal distribution. The total TX linear power can be converted to the dBm scale with

$$P_{tot} = 10\log_{10}\left(P_{\text{lin,tot}}\right) \tag{10}$$

and thus, the total TX power of the TX array on dBm scale closely follows normal distribution.

The detailed RF system design and RF system calculations for the 5G mmW radio transmitter and receiver are presented in [9]. The RF system calculations in [9] have been done with typical values specified in component data sheets as in [24], [25], which is the most common RF system analysis method. The previously presented RF system-level analysis

in [9] has been extended by analyzing the Tx gain variation and the cumulative standard deviation growth on the dB scale along a single Tx path. The result is presented in Fig. 5. The cumulative standard deviation growth is a relative metric. If the standard deviation, and thus the variance for each component (N), is limited, then the cumulative variation will convergence, and the growth of the cumulative variance stagnates.

The standard deviation of 1.0 dB over process-voltage-temperature (PVT) variations for the PA gain was estimated based on the datasheet [26], which leads to the total standard deviation of 2.27 dB for conductive power of each individual TX path. The standard deviation of the radiated TX power from each TX path is 2.35 dB, including the antenna variation is shown in Fig. 5.

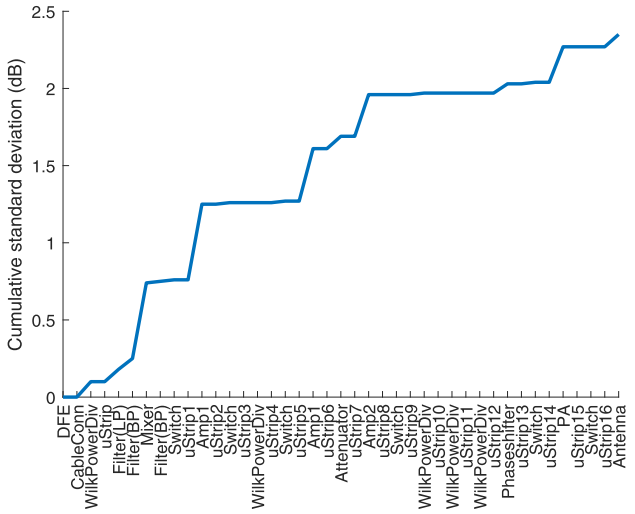

FIGURE 5. Growth of cumulative standard deviation in 5G mmW TX path based on component data sheet values.

Based on the measurements, the range of the conducted TX powers of individual paths is 18.6 dB over the operational frequencies, which corresponds to a 3.11 dB variation with an assumption that the range presents $\pm 3\,\sigma$ variation or the $\boldsymbol{C}_{\mathrm{pk}}$ value is 1.0 [22]. The conductively measured σ of 3.11 dB is significantly larger than the TX system calculated variation σ of 2.27 dB. The TX signal level's variation is due to manufacturing defects of wire bondings of bare die components.

Similar analyses for the mean and the variation are performed for statistical process control purposes when the production process needs to be controlled and maintained within the process control limits. The control limits could be derived from the 5G NR standards in the TX power case. However, the standard specifies only a one sided-limit. Thus, the TX's mean value needs to be set to comply with the standard limit based on the measured σ with the selected quality level.

Monte Carlo (MC) simulations are performed to demonstrate that variation of individual Tx powers will increase the average power from the array transmitter. The MC-simulation model has been done based on system calculation variation

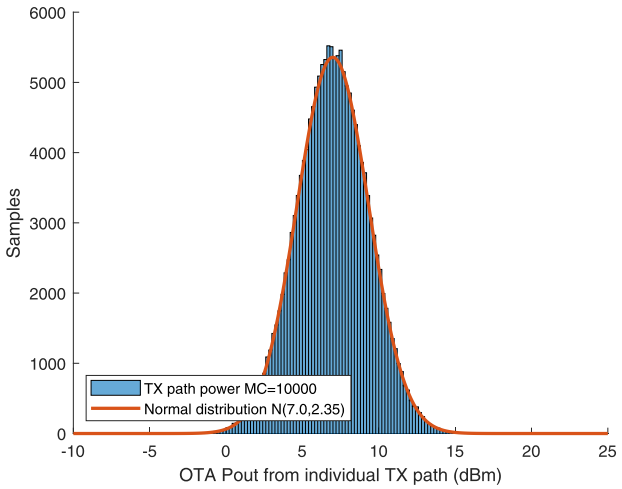

FIGURE 6. MC-simulated (N=10,000) individual TX path radiated power on dBm scale.

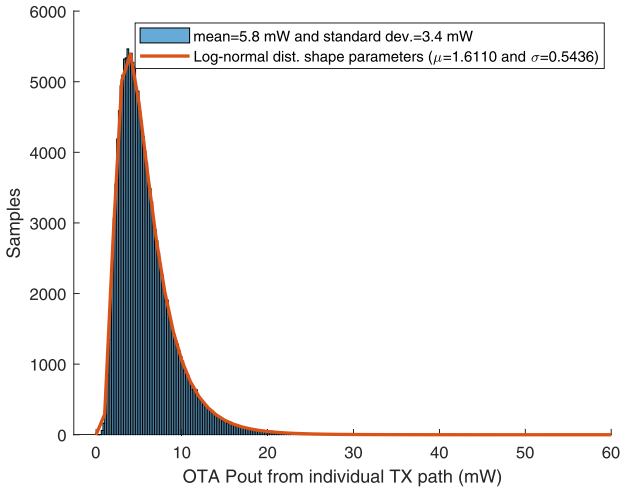

FIGURE 7. Individual TX path radiated power on linear scale and corresponding log-normal distribution based on the MC-simulation (N=10,000).

results shown in Fig. 5 and 10^4 simulation runs are performed. The individual TX path power is assumed to follow normal distribution on the dB scale, and the conductive TX power mean value is 7.0 dBm, which corresponds to total EIRP power of 40.0 dBm from the 16-path Tx array, as shown in the system-level summary Table 1 in sub-section C. The PDF of each TX path's conductive power follows normal distribution on the dBm scale, as shown in Fig. 6. The MC-simulated individual TX powers from the dBm scale have been converted to mW scale values in Fig. 7. TX powers follow a log-normal distribution, and the maximum power is 55.0 mW. In contrast, the mean value is 5.8 mW, and the standard deviation is 3.4 mW. The scale parameters of the log-normal distribution have been calculated with Eqs. (2) and (3).

The implemented 5G mmW radio has 16 TX paths, and the TX level of the array is MC simulated with 10^4 runs.

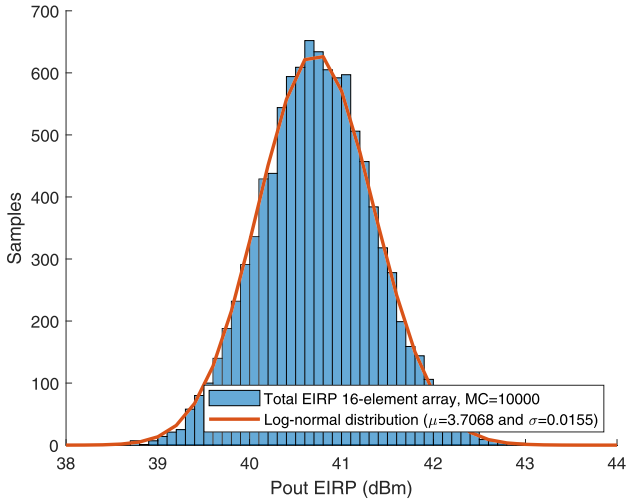

FIGURE 8. OTA combined EIRP of the TX array with the mean of 40.75 dBm and standard deviation of 0.63 dB.

Randomly selected 16 TX OTA signals from the PDF from Fig. 7 have been added together to simulate a perfectly combined TX array signal. The combined TX array OTA signal is converted to dBm scale with (9). It can be seen from Fig. 8 that the mean value of the EIRP increases from 40 dBm to 40.75 dBm calculated based on mean values of components as used in TX system-level calculation. The mean of the array EIRP value increases since some large individual samples of the log-normal distribution significantly impact the total sum of the array TX power, thus increasing the EIRP value. There is no EIRP increase effect if all Tx paths have equal TX power. However, some variation always exists, and the total EIRP increase of the array due to power variations of the individual TX paths is an aspect that should be included in the Tx array system analysis.

Another MC-simulation demonstrates a more significant EIRP shift. The same average TX value of 7.0 dBm is used as in the previous analysis. If the antenna gain variation with $\sigma = 0.59$ dB and the consecutively measured TX variation with $\sigma = 3.11$ dB are combined to the individual TX path OTA variation $\sigma = 3.16$ dB, the TX EIRP is increased to 41.2 dBm with a standard deviation of 0.89 dB.

B. VARIATIONS WITH CALIBRATED TX POWER

The TX power level between different units should be as constant as possible to make each unit fulfill the standard requirements, such as [3], [4]. The TX calibration is done at the production line of mass production with automated test equipment, including TX power level and phase calibration. The TX calibration has two aims: the first aim is to set the average TX power level to the calibration target, and the second aim is to narrow down the part-to-part variation. However, there will always be some variation between products even after the calibration. For LTE and 5G FR1 devices, the calibration is done using conductive measurements, whereas, for 5G mmW (FR2) devices, OTA calibration is preferred.

The TX antenna array's power level varies, and it is limited by the shape of the antenna element's radiation pattern when the beam is steered over the array's electrical beam steering range. The device under test (DUT) is rotated with a rotation table, as shown in Fig. 2. The TX OTA measurement is performed using a fixed reference antenna location. The DUT is physically rotated in the opposite direction with respect to the steering angle during the OTA measurement. In theory, this follows $\cos^1$ relationship with the physical rotation angle [29]. In literature, scanned beam envelopes are reported to follow relationship from $\cos^1$ [30] to $\cos^{1.4}$ [17] at 28 GHz. Additionally, if the rotation center during the measurements is not at the center of the antenna array, it will create an additional amplitude drop over the steering angles.

A progressive phase excitation in the antenna array is required to steer the beam to the desired direction. The electrical beam steering is done in Tx and Rx paths by using phase shifters capable of controlling the phase of mmW signal with 11.25° resolution. Additionally, there is a component-to-component variation of absolute phase change with the same control word. These phase control variations can be calibrated with individual Tx and Rx paths calibration measurements as demonstrated, for example, in [31].

The 5G mmW PoC radio unit's TX phase calibration was performed over a 4 meter OTA link. The TX phase responses across all phase shifter states from each TX branch were characterized with S_{21} S-parameter measurement with a vector signal analyzer connected to the Rx unit. The relative phase calibration method uses full measurement data of phase shifter states from all TX branches to find the best combination of phase shifter states to generate a radiation pattern towards the wanted direction. The absolute phase calibration method uses an average phase error across phase shifter states as a single calibration value for all radiation patterns. The amplitude calibration was done before the phase calibration. The used platform supports individual TX branch amplitude change only by altering the PA's bias to even out the amplitude differences over antenna elements. TX power of each TX branch was OTA measured with a 3.5 m link with a reference RX antenna. The OTA power measurement accuracy was studied with the gage R&R method at a two-meter OTA link for the used antenna array, and a σ of 0.44 dB was measured in [10].

The OTA calibration reduced the measured TX variation down to 0.92 dB over the beam steering values from -15° to 15° [31]. The OTA calibrated normalized TX power levels based on different OTA calibration methods using the phase shifters are shown in Fig. 9(a).

Normalized results are used to concentrate on the variation of TX power due to beam steering phenomena. The absolute mean TX power difference between calibration methods can be calibrated with transmission power control. If these results represent a 5G mmW base station TX level accuracy, and a mobile device is located randomly within the base

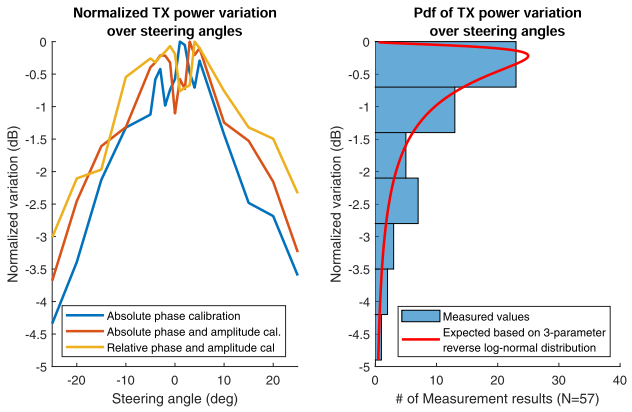

FIGURE 9. Calibrated TX measurements using OTA phase calibration (a) Normalized TX power level over steering angles, and (b) a log-normal PDF of the normalized TX levels with μ of -0.29 dB and σ of 1.20 dB.

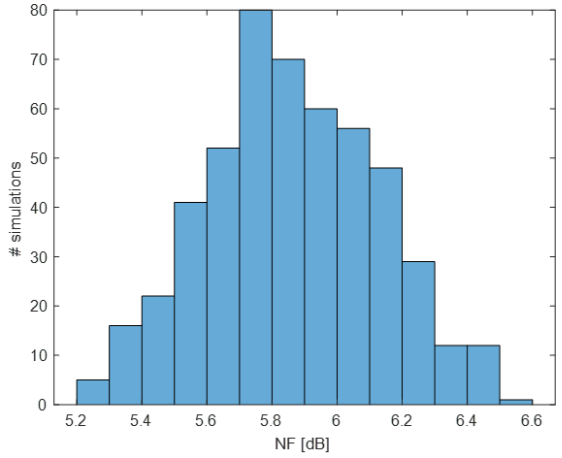

FIGURE 10. PDF of Rx array's NF based on RF system calculation Monte Carlo-simulations using component data sheet variations. The mean is 5.86 dB and σ of 0.26 dB.

station's scan area, then the TX power level would follow the log-normal distribution shown in Fig. 9(b).

C. RECEIVED SIGNAL VARIATION IN RX ARRAY

The 5G mmW PoC uses the same antenna array in both RX and TX operation modes. The Rx array variation includes variations of gain of the antenna element or the 2 × 2 sub-array, a noise figure of the Rx array, and a coherence gain of the Rx array.

The Rx array's NF was measured using the system EVM measurement method, where the system EVM was measured with different RX input power levels. The NF of the Rx array was modeled with noise level raise to match the RX EVM measurements extracted from the system EVM measurements as described in [12]. The measured range of the deviation of the Rx array NF was 1.5 dB corresponding to a σ of 0.25 dB with a (C_{pk} value of 1.0), which matches perfectly with a MC-simulated (N=500) array noise figure σ of 0.26 dB based on component data sheets [33], as shown in Fig. 10. The MC-simulated PDF of the array NF is slightly skewed with a long tail towards high values with a mean value of 5.86 dB. The MC-simulated PDF is not as skewed as expected based on the corner case analysis, where all component variations are set to either minimum or maximum values, as studied in [12]. The MC-analysis includes more typical values into the simulated population than the corner case-based analysis, and thus the skewness is alleviated at the minimum signal level.

An automatic gain control (AGC) maintains the output level at the output of the Rx array constant, even if the signal level in the Rx input varies due to the fading of the mobile channel. The AGC is implemented in the 5G mmW PoC Rx with digitally controlled 1 dB step attenuators. The NF of array Rx is increased when Rx's gain is reduced from the maximum, and skewness of the PDF of the NF is significantly increased towards high values [12].

The RX signal's coherence summation from individual Rx paths is done using Wilkinson power dividers after each Rx path's first LNA. Thus, the coherence gain has some effect on the NF of the Rx array. The coherence gain increases the RX signal power more than the noise level, improving the signal to noise ratio (SNR). The NF increases when the coherence gain decreases, and the implemented 5G mmW PoC is studied using the RX system calculation, and the result is shown in Fig. 11. The Rx array's output level is kept constant at -35 dBm with the AGC functionality, and the used attenuator values are reported in Fig. 11.

The maximum coherence gain gives the minimum NF for the Rx array. If the coherence gain is lower due to the Rx signal phases' mismatches or amplitudes in the coherence summation, the NF of the Rx array is increased. The Rx array's coherence gain was studied in [28], and a range of 3.7 dB was measured. If the range is considered to present

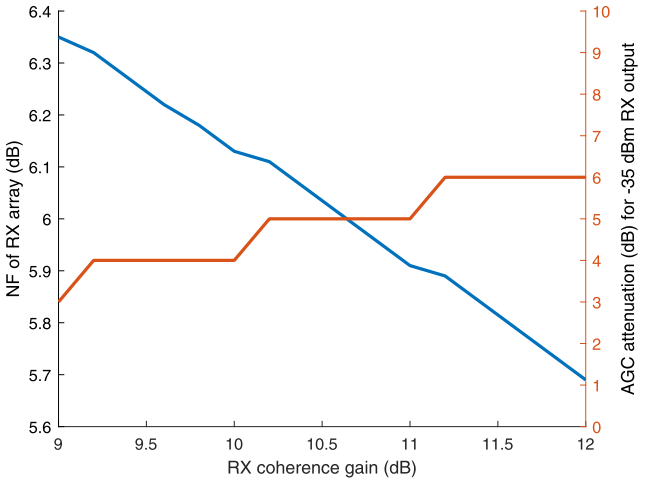

FIGURE 11. Coherence gain reduction increases the NF of the PoC array Rx and a constant level Rx output level is implemented with AGC.

total variation, then $\sigma = 0.61$ dB based on the C_{pk} value of 1.0. The coherence gain variation can be mapped to the variation of Rx array's NF using the blue curve in Fig. 11 and the standard deviation of the NF due to coherence gain is 0.13 dB.

The gain variation of the 2 × 2 sub-array of the used antenna array was measured using a 2 meter OTA link. The average sub-array gain was 9.1 dB with a σ of 0.59 dB. The same antenna array was used in TX and RX units, and thus the same variations apply to both ends of the radio link. The antenna array gain variation is less than the sub-array variation since 16 individual gains are independently summed on a linear scale. The gain variation of the 16-element array was MC-simulated with 10^4 runs resulting σ of 0.13 dB.

The insertion loss (IL) of the RF front-end (RFFE) is estimated to be 2.0 dB based on component datasheets. The RFFE includes two strip lines and one RF switch. The range of IL is 0.40 dB over the PVT variations, which corresponds with σ of 0.07 dB based on C_{pk} value of 1.0 assumption.

Two different methods to calculate the Rx array sensitivity are shown in Table 1. The first method is to calculate the Rx array sensitivity based on the RF system parameters shown at rows A to M in Table 1. The Rx sensitivity variation on row N includes the antenna array gain variation (row C), variation of the Rx NF (row L), and NF variation due to the coherence gain variation (0.13 dB), yielding a combined σ of 0.31 dB.

The second method to calculate the RF sensitivity is to use an RF system calculation spreadsheet based on average RF component values. The Rx sensitivity based on the RX system calculation [9] is presented on row T. The variation of Rx sensitivity in the spreadsheet calculation is only due to the variation of NF, which is shown in Fig. 10.

The OTA sensitivity measurement result was measured with the system EVM measurement performed inside the EMC-chamber over a 3.5 m OTA link using 5G NR 16-QAM signal [12]. The mean and the variation of OTA measured Rx sensitivities are calculated based on beam steering results from −15° to 15° in the boresight direction of the DUT, and results are shown on row R in Table 1.

An excellent agreement with the OTA measurements and two Rx sensitivity calculation methods can be seen from Table 1. All measured and calculated RX sensitivities using 5G NR 16-QAM modulation are within one decibel. The mean values of the RF system calculated and OTA EVM measured 16-QAM modulation values are even statistically similar based on a two-sample t-test with 95% confidence. The OTA EVM measured link range of the 16-QAM passes the two-sample t-test with 95% confidence with both the link ranges based on the RF system calculation and the measured parameter estimated range.

TABLE 1. System Level calculations of 5G mmW PoC with 5G NR 16-QAM with the calibrated TX power of 40 dBm.

Row	Parameter	Mean	Range	σ	Unit	Ref
A	Sub-arrays in the whole array	16/12.0			lin/dB	
B	OTA measured gain of sub-array	9.1		0.59	dB	
C	OTA antenna array gain (A + B)	21.0		0.13	dBi	
D	Modulation BW	98.0			MHz	[28]
E	Noise density power	-174.23			dBm/Hz	
F	Noise at BW (D + E)	-94.32			dBm	
G	Rx SNR req. at output	15.17			dB	[12]
H	Conducted Pout each TX path (FE losses incl.)	7.0		2.35	dBm	Fig.6
I	Mean value RF system calc. TX EIRP (C+H+A)	40.0			dBm	
J	MC-simul. TX EIRP (based on H)	40.75		0.63	dBm	Fig.8
K	Measured TX EIRP	**40.0**		0.44	dBm	[10]
L	Measured Rx array's NF	5.0	1.5	0.25	dB	[12]
M	Meas. Rx coherence gain	11.0	3.70	0.61	dB	[28]
N	Measurement based Rx array sens. (F+G+L)	**-74.15**		0.31	dBm	
O	Link budget (K-N)	114.15		0.54	dB	
P	Path loss coefficient	2.0			lin	[32]
Q	Calculated distance	434.4		15.3	m	
	OTA system EVM method					
R	Rx sensitivity over beam steering	**-73.7**		0.54	dBm	[12]
S	Dist. based EVM meas.	414.7		25.8	m	
	Data sheet values					
T	RF system calc. Rx sens.	**-73.6**		0.26	dBm	Fig.10
U	Distance from RF system calc.	410.0		12.2	m	

IV. ARRAY SYSTEM PATHLOSS CALCULATION AND UNCERTAINTY

The cell boundary in the telecommunication system is not a fixed line but more a statistical value around the calculated mean value. The cell area's uncertainty and the cell coverage based on a mathematical path loss model are analyzed in [34]. A link range analysis based on RF system-level parameters for carrier-grade Wi-Fi at 2.4 GHz is presented in [35], and for 5G mmW system, adaptive modulations with multiple beams in [36]. These analyses assume a stabile RF performance or that there is no variation between units. However, there is always a product-to-product variation present due to a component-to-component variation.

The initial link range analysis for the 5G mmW PoC radio based on selected components' mean values has been presented in [28]. The initial RF system analyses expected that the EIRP of the TX array could be 60 dBm in [9] and [28]. The maximum OTA measured EIRP of 45 dBm was measured from the 5G mmW PoC due to implementation imperfections and use of wire-bonded bare die components [12]. The TX EIRP power was set at 40 dBm during the OTA measurements in the EMC-chamber to avoid the RX unit's compression.

The variances of measured EIRP (row K) and the Rx sensitivity (row N) are combined, resulting in the total link range σ of 0.54 dB (row O). The estimated link ranges based on the simulation parameters and OTA EVM measurements have a good agreement for the studied 16-QAM modulation in Table 1.

The estimated link range variation can be calculated based on the link budget variation using the MC-simulation. The range for a line of sight (LOS) radio link can be calculated

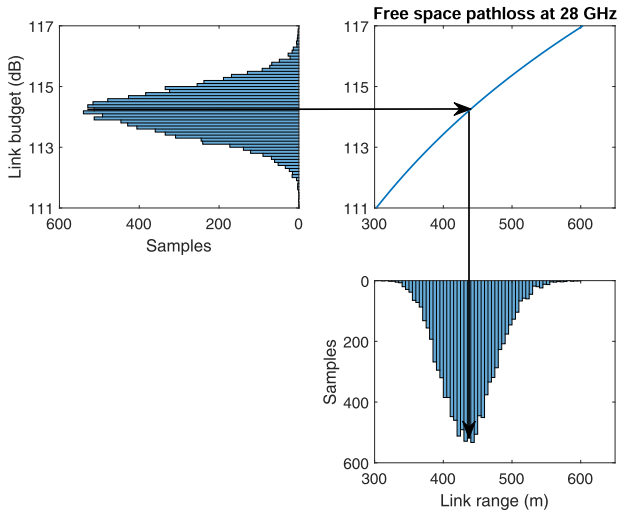

FIGURE 12. MC-simulated link budget (Table 1; row N) mapping to LOS link range distance (N=10,000).

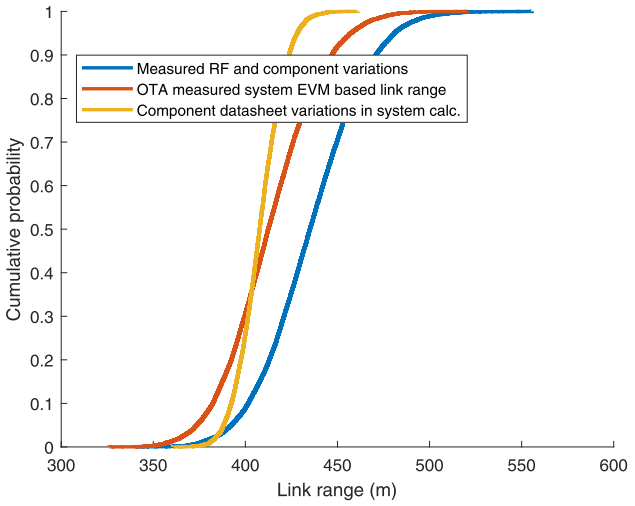

FIGURE 14. MC-simulated CDF of link ranges based on measurements and RF system analysis (N=10,000).

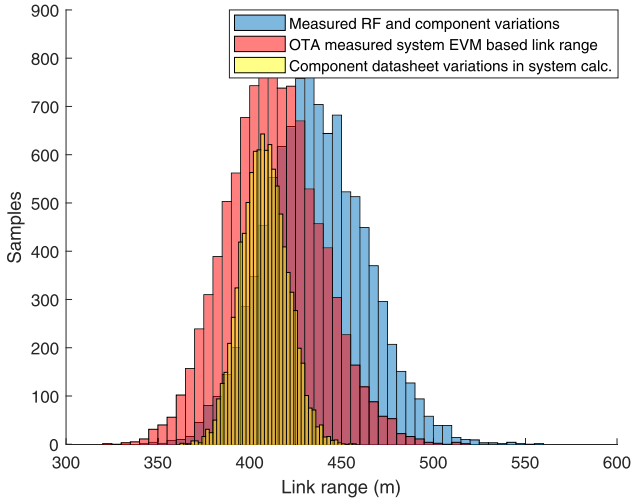

FIGURE 13. MC-simulated PDFs of link ranges based on measurements and RF system analysis (N=10,000).

based on the free space path loss equation, and it can be derived into the following form [27]:

$$R = 10^{(FSPL - 20\log_{10}(f) + 147.55)/20} \tag{11}$$

where FSPL is a free-space path loss in dB, and f is the frequency in Hz. Thus, Eq. (11) acts as a mapping function of the PDF of the link budget, which has a standard deviation of 0.54 dB based on measured variations. It can be seen from Fig. 12 that the free-space loss function is non-linear, and thus it shapes the PDF of the link budget to the PDF of the link range. The MC-simulated (10^4 runs) PDF of the link budget closely follows the normal distribution, while the PDF of the link range follows the log-normal distribution with a tail towards large values. The non-linearity of the free space loss function increases when the link budget increases.

The probability density functions link range estimates based on the RF system calculation using component datasheet PVT variations, measured variation in conductive measurements, and OTA measured system EVM are presented in Fig. 13. It can be seen from Fig. 13 that all link range estimates follow the log-normal distribution. However, the maximum link range estimation differs significantly due to the log-normal shapes of the PDFs. However, each distribution has different shapes due to different mean and standard deviation values.

The cumulative probability density functions (CDFs) of the link range estimates are shown in Fig. 14. The 50% percentiles of the distributions or the mean values are close to each other, even statistically matching. It can be observed that the components' datasheet values-based RF system calculation and the OTA measured system EVM link range have the same link range estimate if the 90% percentile of the link ranges (or 10% link outage probability) are studied.

V. CONCLUSION

A statistical study of RF parameters is needed to predict radio system performance, such as coverage area and data rate accurately. Statistical information is also needed for quality assurance purposes during the product development and manufacturing phases. If the statistical distributions of the RF components and RF system-level parameters and their relationship are known, then the radio system performance can be optimized.

We showed that individual path TX powers' mean and variance affect the increase of the EIRP of the array compared with the EIPR calculated using average values of individual TXs. It was reported that used component tolerances in the 5G mmW PoC radio could increase the array's EIRP by 0.75 dB in RF system calculation compared to the calculation using average values without variability. An improvement of 1.2 dB

EIRP is expected based on measured variations of individual TX path powers without TX calibrations.

The RX signal combination from multiple individual paths in the Rx array is performed using electrical components such as Wilkinson power dividers. These components have part-to-part and frequency response variations, which will affect the achieved Rx coherence gain. The coherence gain reduction from the maximum gain increases the noise figure of the array receiver. This effect was analyzed in the paper with RF system calculations and Monte Carlo simulations and a measured coherence gain range 3.7 dB maps to array noise figure range of 0.8 dB.

A worst-case part-to-part analysis can be done at the RF system-level calculations by combining the components' minimum and maximum values. If statistical distributions of each parameter are known then, Monte Carlo-simulations can be performed, giving a more presentative behavior of the analyzed parameter. The NF of the 5G PoC Rx array has been MC-simulated with RF system-level calculations, and the simulated and the OTA measured values have an excellent match.

This paper proves that a normally distributed link budget on the dB scale maps via a non-linear mapping function to a log-normally distributed link range. The non-linearity of the mapping function increases with increasing link budget values on the dB scale, expanding the tail of the distribution towards large values. The log-normal behavior of the 5G mmW link range, due to device-to-device and TX power fluctuations over the steering angles of the base station and user equipment, needs to be taken into account the network planning of coming 5G networks, especially outdoors.

Similar link range estimates can be achieved with an RF system calculation based on the component datasheet values or the RF system-level parameter study. Both estimates have been validated with a short-range OTA measurement within the EMC-chamber using system EVM measurement methodology without a cumbersome outdoor measurement campaign. The estimated Rx array sensitivities and OTA measured values are within one dB, which is an excellent match.

REFERENCES

[1] *5G Implementation Guideline, Version 2.0*, GSM Association, London, U.K., Jul. 2019.

[2] *NR; Study on Integrated Access and Backhaul (Release 16)*, document (TR) 38.874, 3GPP, Version 16.0.0, Dec. 2018. Accessed: Oct. 12, 2020. [Online]. Available: https://portal.3gpp.org/

[3] *User Equipment (UE) Radio Transmission and Reception, Part 2: Range 2 Standalone (Release 15)*, document 3GPP TS 38.101-2 V15.4.0, Dec. 2018. Accessed: Oct. 12, 2020. [Online]. Available: https://portal.3gpp.org/

[4] *Base Station (BS) Radio Transmission and Reception (Release 15)*, document 3GPP TS 38.104 V15.4.0, Dec. 2018. Accessed: Oct. 12, 2020. [Online]. Available: https://portal.3gpp.org/

[5] K. Khalaf, K. Vaesen, S. Brebels, G. Mangraviti, M. Libois, C. Soens, and P. Wambacq, "A 60 GHz 8-way phased array front-end with TR switching and calibration-free beamsteering in 28 nm CMOS," in *Proc. 43rd IEEE Eur. Solid State Circuits Conf. (ESSCIRC)*, Sep. 2017, pp. 203–206.

[6] A. Natarajan, S. K. Reynolds, M. D. Tsai, S. T. Nicolson, J.-H. C. Zhan, D. G. Kam, D. Liu, Y.-L. O. Huang, A. Valdes-Garcia, and B. A. Floyd, "A fully-integrated 16-element phased-array receiver in SiGe BiCMOS for 60-GHz communicationsan," *IEEE J. Solid-State Circuits*, vol. 46, no. 5, pp. 1059–1075, Apr. 2011.

[7] K. Kibaroglu, M. Sayginer, T. Phelps, and G. M. Rebeiz, "A 64-element 28-GHz phased-array transceiver with 52-dBm EIRP and 8–12-Gb/s 5G link at 300 meters without any calibration," *IEEE Trans. Microw. Theory Techn.*, vol. 66, no. 12, pp. 5796–5811, Dec. 2018.

[8] K. Kibaroglu, M. Sayginer, and G. M. Rebeiz, "A low-cost scalable 32-element 28-GHz phased array transceiver for 5G communication links based on a 2 × 2 beamformer flip-chip unit cell," *IEEE J. Solid-State Circuits*, vol. 53, no. 5, pp. 1260–1274, May 2018.

[9] O. Kursu, M. E. Leinonen, G. Destino, N. Tervo, M. Sonkki, T. Rahkonen, A. Pärssinen, S. Tammelin, M. Pettissalo, and A. Korvala, "Design and measurement of a 5G mmW mobile backhaul transceiver at 28 GHz," *EURASIP J. Wireless Commun. Netw.*, vol. 2018, no. 1, pp. 1–11, Aug. 2018.

[10] M. E. Leinonen, M. Sonkki, and A. Pärssinen, "Statistical measurement system analysis of over-the-air measurements of antenna array at 28 GHz," in *Proc. 12th Eur. Conf. Antennas Propag. (EuCAP)*, London, U.K., 2018, pp. 1–5.

[11] M. E. Leinonen, N. Tervo, M. Sonkki, and A. Parssinen, "Quality analysis of antenna reflection coefficient in massive MIMO antenna array module," in *Proc. 15th Eur. Radar Conf. (EuRAD)*, Madrid, Spain, Sep. 2018, pp. 1553–1556.

[12] M. E. Leinonen, M. Jokinen, N. Tervo, O. Kursu, and A. Pärssinen, "System EVM characterization and coverage area estimation of 5G directive mmW links," *IEEE Trans. Microw. Theory Techn.*, vol. 67, no. 12, pp. 5282–5295, Dec. 2019.

[13] M. E. Leinonen, "Usage of process capability indices during development cycle of mobile radio product," in *Systems Engineering: Practice and Theory*, B. Cogan, Ed. Rijeka, Croatia: IntechOpen, Mar. 2012.

[14] F. W. Breyfogle, *Implementing Six Sigma*. Hoboken, NJ, USA: Wiley, 1999.

[15] M. Wiles and V. Rodriguez, "Choosing the right chamber for your test requirements," *Interference Technol., Int. J. Electromagn. Compat.*, pp. 32–49, May 2010.

[16] M. Sonkki, S. Myllymäki, N. Tervo, M. E. Leinonen, M. Sobocinski, G. Destino, and A. Pärssinen, "Linearly polarized 64-element antenna array for mm-Wave mobile backhaul application," in *Proc. 12th Eur. Conf. Antennas Propag. (EuCAP)*, London, U.K., 2018, pp. 1–5.

[17] B. Rupakula, S. Zihir, and G. M. Rebeiz, "Low complexity 54–63-GHz transmit/receive 64-and 128-element 2-D-scanning phased-arrays on multilayer organic substrates with 64-QAM 30-Gbps data rates," *IEEE Trans. Microw. Theory Techn.*, vol. 67, no. 12, pp. 5268–5281, Dec. 2019.

[18] J. Li, Y. Qi, W. Yu, F. Li, J. Fan, Z. Yang, S. Wu, and J. L. Drewniak, "Total isotropic sensitivity measurement in switched beam antenna systems," *IEEE Trans. Instrum. Meas.*, vol. 69, no. 8, pp. 5458–5467, Aug. 2020.

[19] J. S. Hurtarte and M. Wen, "Over-the-air testing for 5G mmWave devices: DFF or CATR?" *Microw. RF*, , vol. 58, no. 3, pp. 36–38, Mar. 2019.

[20] Anritsu Corporation, "5G solution catalog 2020 summer," Anritsu Corporation, Kanagawa, Japan, Catalog 5G-Solution-E-A-1-(3.00), Jul. 2020, p. 12.

[21] E. J. Dudewich and S. N. Mishra, *Modern Mathematical Statistics*. Hoboken, NJ, USA: Wiley, 1988, p. 838.

[22] AIAG, "Measurement system analysis (MSA)," in *Reference Manual*, 4th ed. Lansing, MI, USA: Automotive Industry Action Group (AIAG), 2010, p. 752.

[23] N. L. Jonhson, S. Kotz, and N. Balakrishnan, *Continous Univariate Distributions*, 2nd ed., vol. 1. Hoboken, NJ, USA: Wiley, 1994.

[24] Analog Devices, "HMC264LC3B GaAs MMIC sub-harmonic SMT mixer 21—31 GHz," Data Sheet HMC264LC3B, V04.0414, Analog Devices, Norwood, MA, USA, Nov. 2017.

[25] Marki Microwave, PD-0530SMG 5—30 GHz power divider," Data Sheet PD-0530SMG, Marki Microwave, Morgan Hill, CA, USA, Nov. 2018.

[26] Qorvo, "TGA2595 27.5–31 GHz 9 W GaN power amplifier," Data sheet TGA2595, Rev. B, Qorvo, Greensboro, NC, USA, Oct. 2018.

[27] C. A. Balanis, *Antenna Theory: Analysis and Design*, 3rd ed. Hoboken, NJ, USA: Wiley, 2005.

[28] M. E. Leinonen, G. Destino, O. Kursu, M. Sonkki, and A. Pärssinen, "28 GHz wireless backhaul transceiver characterization and radio link budget," *ETRI J.*, vol. 40, no. 1, pp. 89–100, Feb. 2018.

[29] R. J. Mailloux, *Phased Array Antenna Handbook* (Artech House Antennas and Propagation Library), 2nd ed. Norwood, MA, USA: Artech House, 2005.
[30] A. Nafe, M. Sayginer, K. Kibaroglu, and G. M. Rebeiz, "2 × 64-element dual-polarized dual-beam single-aperture 28-GHz phased array with 2 × 30 Gb/s links for 5G polarization MIMO," *IEEE Trans. Microw. Theory Techn.*, vol. 68, no. 9, pp. 3872–3884, Jun. 2020.
[31] M. Jokinen, O. Kursu, N. Tervo, J. Saloranta, M. E. Leinonen, and A. Parssinen, "Over-the-air phase measurement and calibration method for 5G mmW phased array radio transceiver," in *Proc. 93rd ARFTG Microw. Meas. Conf. (ARFTG)*, Boston, MA, USA, Jun. 2019, pp. 1–4.
[32] D. He, B. Ai, M. Schmieder, Z. Zhong, J. Kim, B. Hui, H. Chung, I. Kim, and Y. Hao, "Influence analysis of typical objects in rural railway environments at 28 GHz," *IEEE Trans. Veh. Technol.*, vol. 68, no. 3, pp. 2066–2076, Mar. 2019.
[33] M. E. Leinonen, "Over-the-air measurements, tolerances and multiradio interoperability on 5G mmW radio platform," Ph.D. dissertation, Dept. Elect. Eng., Oulu Univ., Oulu, Finland, 2020.
[34] P. Bernardin, M. F. Yee, and T. Ellis, "Cell radius inaccuracy: A new measure of coverage reliability," *IEEE Trans. Veh. Technol.*, vol. 47, no. 4, pp. 1215–1226, Nov. 1998.
[35] A. Adler and M. Salhov, "A carrier-grade wireless lan network implementation [application notes]," *IEEE Microw. Mag.*, vol. 9, no. 4, pp. 108–119, Aug. 2008.
[36] T. Tuovinen, N. Tervo, and A. Parssinen, "Analyzing 5G RF system performance and relation to link budget for directive MIMO," *IEEE Trans. Antennas Propag.*, vol. 65, no. 12, pp. 6636–6645, Dec. 2017.

MARKO E. LEINONEN (Member, IEEE) received the M.Sc., Licentiate in Technology, and Doctor of Science degrees in electrical engineering from the University of Oulu, Oulu, Finland, in 1996, 2002, and 2020, respectively. From 1994 to 2012, he was with Nokia Mobile Phones, Oulu, working with various positions with radio engineering and technology management. From 2006 to 2007, he was a Senior Engineering Manager in Bengaluru, India. From 2012 to 2016, he was a Master Developer with Ericsson, Oulu. Since 2017, he has been with the Centre for Wireless Communications, University of Oulu, where he is currently a Research Manager. He holds 40 granted international patent families concentrating on radio engineering. His research interests include wireless radio systems and quality topics in radio engineering.

NUUTTI TERVO (Member, IEEE) received the B.Sc. (Tech.) and M.Sc. (Tech.) degrees in electrical engineering from the University of Oulu, in 2014, where he is currently pursuing the Ph.D. degree with the Centre for Wireless Communications (CWC) Research Unit. He has a strong background in different fields of wireless communications, including RF, radio channel modeling, signal processing, and system-level analysis. Around those topics, he has authored or coauthored 35 international journal and conference papers. His PhD dissertation research focuses on nonlinearity and linearization of millimeter-wave beamforming transceivers.

MARKKU JOKINEN received the M.Sc. degree in electronics from the University of Oulu, in 2010. He is currently pursuing the Ph.D. degree. He is also working as a Research Scientist with the Centre for Wireless Communications, University of Oulu. He has been recently focusing on the measurement techniques. He has gained experience on the design and implementation of wireless system algorithms and protocols with software-defined radio platforms.

OLLI KURSU received the M.Sc. and D.Sc. degrees in electrical and electronics engineering from the University of Oulu, Oulu, Finland, in 2006 and 2015, respectively. He is currently working as a Postdoctoral Researcher with the Centre for Wireless Communications, University of Oulu. His research interests include mmW, RF, and analog and mixed signal circuit design for wireless communication systems.

AARNO PÄRSSINEN (Senior Member, IEEE) received the M.Sc., Licentiate in Technology, and Doctor of Science degrees in electrical engineering from the Helsinki University of Technology, Finland, in 1995, 1997, and 2000, respectively. From 1994 to 2000, he was with the Electronic Circuit Design Laboratory, Helsinki University of Technology, working on direct conversion receivers and subsampling mixers for wireless communications. From 2000 to 2011, he was with the Nokia Research Center, Helsinki, Finland. From 2011 to 2013, he was working as a Distinguished Researcher and RF Research Manager with Renesas Mobile Corporation, Helsinki. From October 2013 to September 2014, he was an Associate Technical Director with Broadcom, Helsinki. Since September 2014, he has been with the Centre for Wireless Communications, University of Oulu, Oulu, Finland, where he is currently a Professor. He has authored or coauthored one book, one chapter of a book, more than 150 international journal and conference papers and holds several patents. His research interests include wireless systems and transceiver architectures for wireless communications with special emphasis on the RF and analog integrated circuit and system design.